Calculated Spectroscopy and Atmospheric Photodissociation of Phosphoric Acid

ARTICLE *in* THE JOURNAL OF PHYSICAL CHEMISTRY A · JULY 2010

Impact Factor: 2.69 · DOI: 10.1021/jp1007957 · Source: PubMed

4 AUTHORS, INCLUDING:

Joseph Lane
The University of Waikato
43 PUBLICATIONS **639** CITATIONS
SEE PROFILE

Henrik G Kjaergaard
University of Copenhagen
141 PUBLICATIONS **3,834** CITATIONS
SEE PROFILE

Calculated Spectroscopy and Atmospheric Photodissociation of Phosphoric Acid

Mivsam Yekutiel

Department of Chemistry, University of Otago, P.O. Box 56, Dunedin 9054, New Zealand

Joseph R. Lane

Department of Chemistry, University of Waikato, Private Bag 3105, Hamilton 3240, New Zealand

Priyanka Gupta

Department of Chemistry, University of Otago, P.O. Box 56, Dunedin 9054, New Zealand

Henrik G. Kjaergaard*

Department of Chemistry, University of Copenhagen, Universitetsparken 5, DK-2100 Copenhagen Ø

Received: January 27, 2010; Revised Manuscript Received: May 18, 2010

Detection of phosphine (PH_3) gas in the upper troposphere suggests that the biogeochemical P cycle also includes an atmospheric component that consists of volatile phosphorus-containing molecules. A reasonable end product for the oxidation of PH_3 in the atmosphere is phosphoric acid (H_3PO_4). We propose that H_3PO_4 may be photodissociated into $HOPO_2$ and H_2O in the stratosphere, where H_3PO_4 is likely to be present in gaseous form. We have calculated the energy barrier of this reaction and show that in addition to electronic transitions, OH-stretching overtone transitions can also provide the necessary energy. OH-stretching fundamental and overtone transitions were calculated with the use of an anharmonic oscillator local mode model. The probability of overtone induced photodissociation was estimated with molecular dynamical reaction coordinate simulations. Electronic transitions were calculated with the equation of motion coupled cluster singles doubles method. We have calculated the photodissociation rate constants for absorption of visible, UV, and Lyman-α radiation at altitudes from 20 to 100 km. We show that at altitudes between 30 and 70 km, the photodissociation of H_3PO_4 is likely to proceed via absorption in the UV region by electronic transitions.

Introduction

Phosphorus (P) is an element that is vital to the life of all organisms and is often a limiting nutrient in the natural environment.[1−3] However, current biogeochemical models of the P cycle include only phosphate compounds.[4,5] In 2003, Glindenmann et al. detected phosphine gas (PH_3) in the upper troposphere at altitudes up to 12 500 m.[6] This result clearly questions the current exclusion of volatile phosphorus compounds from biogeochemical models.[7,8] Recently, it has been suggested that ∼10% of the estimated 4.3 Tg/year of global atmospheric flux of phosphorus could be linked to phosphine gas.[9] Altough phosphine is known to be reactive in air, the flammability limit of phosphine is on the order of grams per cubic meter, which is significantly higher than the trace amounts (nanograms per cubic meter or less) detected in the atmosphere.[6,10−12] Phosphine has also been detected in the natural environment 220 days after it was used for fumigation of wheat,[13] suggesting that it has a reasonable stability in the atmosphere. For these reasons, we conclude that it is highly likely that there is an atmospheric component to the biogeochemical P cycle that includes volatile P-containing compounds.

In phosphine, P is in its most reduced form, and due to the oxidizing nature of Earth's atmosphere, compounds with the formula O_yPH_x are certain to exist. It follows that through a series of reactions, PH_3 is likely be oxidized to form phosphoric acid (H_3PO_4), in which phosphorus is in its highest oxidation state.[14] Phosphoric acid is very hygroscopic[15] and, hence, at lower altitudes (<30 km) is likely to exist in aerosols, whereas at higher altitudes, it is likely to be present in gaseous form. This partition between aerosols and gas phase is similar to that of sulfuric acid, which is known to exist in Earth's atmosphere up to 80 km.[16] We suggest that understanding the properties of phosphoric acid is a sensible first step in developing the atmospheric component of the biogeochemical cycle of phosphorus. It was recently proposed that the photodissociation of sulfuric acid in the stratosphere occurs via a vibrational overtone excitation mechanism and not via UV absorption, as previously assumed.[17,18] It is an exciting possibility that photodissociation of phosphoric acid (to form $HOPO_2$ and H_2O) could occur in the atmosphere, similar to what was found for sulfuric acid.

In this paper, we present a theoretical study of the spectroscopy and likely atmospheric photodissociation of gaseous phosphoric acid. We present vibrational and electronic spectra of H_3PO_4 calculated using high level ab initio methods and correlation consistent basis functions. We discuss the dissociation of H_3PO_4 into $HOPO_2$ (metaphosphoric acid) and H_2O and consider three possible photodissociation mechanisms. Finally, we calculate photodissociation rate constants to assess which photodissociation mechanism is likely to dominate at a given altitude.

* To whom correspondence should be addressed. Phone: 45-35320334. Fax: 45-35320322. E-mail: hgk@kiku.dk.

10.1021/jp1007957
Published on Web 06/28/2010

Theory and Calculations

We have optimized the geometry of the reactant, transition state, and products of the photodissociation reaction of H_3PO_4 using the Møller−Plesset second-order perturbation (MP2) and coupled cluster singles and doubles and perturbative triple excitations [CCSD(T)] methods combined with the aug-cc-pV(T+d)Z basis set. For the transition state optimization, we used the MP2/aug-cc-pV(T+d)Z Hessian and the CCSD(T)/aug-cc-pV(T+d)Z first-order energy derivatives.

All MP2 and CCSD(T) calculations assume a frozen core (O: 1s; P: 1s,2s,2p) and were performed with Molpro 2006.1.[19] The optimization threshold criteria were set to step $=1 \times 10^{-6}$ a.u., grad $= 1 \times 10^{-6}$ a.u., energy $= 1 \times 10^{-8}$ a.u. Single-point energy criteria were set to orbital $= 1 \times 10^{-9}$ a.u., coeff $= 1 \times 10^{-9}$ a.u., energy $= 1 \times 10^{-9}$ a.u.

To calculate the relative energetics of the photodissociation reaction of H_3PO_4, we have extrapolated the ground state electronic energy to the complete basis set (CBS) limit with the following two parameter extrapolation for the correlation energy:

$$E_{XY}^{\mathrm{corr}} = \frac{X^3 E_X^{\mathrm{corr}} - Y^3 E_Y^{\mathrm{corr}}}{X^3 - Y^3} \tag{1}$$

where X and Y are the cardinal numbers of the two basis sets and E_X^{corr} and E_Y^{corr} are the corresponding correlation energies obtained with the CCSD(T) method.[20,21] The extrapolated correlation energy, E_{TQ}^{corr} is added to the HF/aug-cc-pV(Q+d)Z energy to give an estimate of the CCSD(T)/CBS energy. All energies are obtained at the CCSD(T)/aug-cc-pV(T+d)Z geometries. We have performed thermodynamical corrections for all the species involved in the photodissociation reaction using MP2/aug-cc-pV(T+d)Z harmonic frequencies and rotational constants. We have calculated anharmonic fundamental frequencies of H_3PO_4 using the standard Rayleigh−Schrödinger vibrational second-order perturbation theory (VPT2)[22] with the MP2/aug-cc-pV(T+d)Z method as implemented in Gaussian 03.[23] We have also calculated CCSD(T)/aug-cc-pV(T+d)Z harmonic frequencies for H_3PO_4 using Molpro 2006.1.[19]

We have calculated the OH-stretching frequencies and oscillator strengths for H_3PO_4 within the local mode model.[24] The OH-stretching vibration is considered isolated from the other vibrational modes.[24−27] This is a good approximation for the calculation of vibrational overtone spectrum because the local modes carry nearly all the intensity.[28] Coupling to other modes has the effect of altering the band profile but has generally little effect on the overall intensity. The 1D Schrödinger equation is solved with two different approaches.[29] The first approach describes the OH-stretching local mode by a Morse potential with the vibrational energy levels given by

$$E(v)/(hc) = \left(v + \frac{1}{2}\right)\tilde{\omega} - \left(v + \frac{1}{2}\right)^2 \tilde{\omega}x \tag{2}$$

and the associated well-known Morse oscillator wave functions.[30] The Morse oscillator frequency, $\tilde{\omega}$, and anharmonicity, $\tilde{\omega}x$, are found from the second-, third-, and fourth-order derivatives of the potential energy curve as described previously.[31,32] These derivatives are found by fitting a 14th-order polynomial to a 15-point ab initio calculated potential energy curve, obtained by displacing the OH bond from −0.3 to 0.4 Å in 0.05 Å steps around equilibrium.[33,34] In the second approach, the 1D Schrödinger equation is solved numerically using a finite element method to give both the vibrational energy levels and wave functions.[35] The potential energy curve used for this numeric approach covers the range from −0.3 to 0.6 Å in 0.025 Å steps around equilibrium. This ensures a converged energy level and wave functions, as shown in previous work.[36] The dimensionless oscillator strength, f, of a transition from the vibrational ground state, $|0\rangle$, to a vibrationally excited state, $|v\rangle$, is given by[37,38]

$$f_{v0} = 4.702 \times 10^{-7}[\mathrm{cm\ D^{-2}}]\tilde{\nu}_{v0}|\vec{\mu}_{v0}|^2 \tag{3}$$

where $\tilde{\nu}_{v0}$ is the vibrational frequency of the transition in $\mathrm{cm^{-1}}$, and $\vec{\mu}_{v0} = \langle v|\vec{\mu}|0\rangle$ is the transition dipole moment matrix element in Debye (D). The dipole moment function is approximated by a series expansion in the internal OH-stretching displacement coordinate about the calculated equilibrium geometry.[18] We fit a sixth-order polynomial to a 15-point dipole moment function from −0.3 to 0.4 in 0.05 Å steps around equilibrium.

We have studied the dynamics of the dissociation reaction of H_3PO_4 into $HOPO_2$ and H_2O by classical trajectory calculations. We have performed "on-the-fly" molecular dynamical reaction coordinate (DRC)[39] simulations, as implemented in GAMESS.[40,41] We adopt a similar sampling procedure and level of theory to that previously used by Miller et al. to describe the OH-stretching overtone induced photodissociation of nitric acid (HNO_3) and sulfuric acid (H_2SO_4).[42,43] We used the correlation-corrected vibrational self-consistent (CC-VSCF) method to compute the initial energy level and wave functions of the OH-stretching overtones of H_3PO_4.[44,45] VSCF and CC-VSCF methods have been previously shown to give calculated fundamental, overtone, and combination-mode transitions that compare well with experiment.[42,46,47] The CC-VSCF method incorporates anharmonic and pairwise mode−mode coupling corrections that are important for the description of high vibrational excited states in a normal mode basis.[44,45] The potential energy surfaces used both in the CC-VSCF and in the classical trajectory calculations were from the PM3 electronic structure algorithm.[48,49] This semiempirical method compares less well with spectroscopy experiments than ab initio methods, such as MP2 and CCSD(T), but experience with similar systems indicates that these potential surfaces are at least semiquantitively valid.[42,43] To ensure total energy conservation, each trajectory is calculated with a small time step of 0.08 fs for a maximum elapsed time of 200 ps.

We have calculated vertical excitation energies and oscillator strengths of H_3PO_4 with the equation of motion-coupled cluster singles doubles (EOM-CCSD) method using the aug-cc-pV(T+d)Z and aug-cc-pV(T+d)Z+5 basis sets. The +5 notation indicates additional primitive basis functions originating from the center of mass. These basis functions were generated according to the procedure by Kaufmann et al. and were used to ensure saturation of diffuse basis functions for some of the highly delocalized Rydberg excited states.[50,51] We have chosen a set of 5s5p5d functions with "semiquantum numbers" from 2.0 to 4.0, in half-integral steps.

Results and Discussion

We find the lowest-energy conformer of H_3PO_4 to have C_3 symmetry, and we show this conformer in Figure 1. To our knowledge, the structure of phosphoric acid in the gas phase has yet to be determined experimentally. In Table 1, we compare our calculated geometric parameters with the available crystal

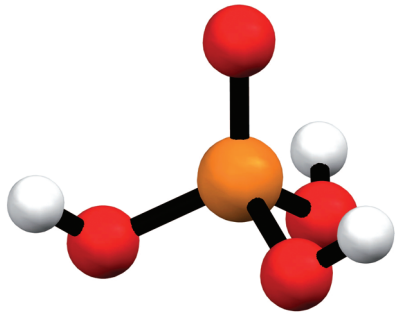

(a) C_3 conformer

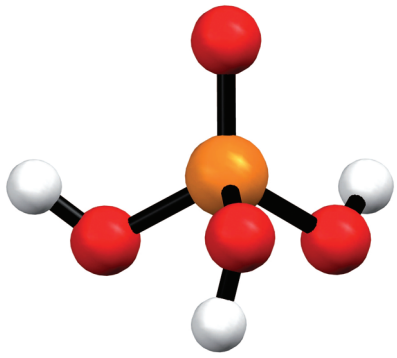

(b) C_1 conformer

Figure 1. CCSD(T)/aug-cc-pV(T+d)Z optimized structures of H_3PO_4. The C_3 conformer is ~1.5 kcal mol^{-1} lower in energy than the C_1 conformer.

TABLE 1: Selected Geometric Parameters of H_3PO_4 (in angstroms and degrees)

parameter	MP2[a]	CCSD(T)[a]	experiment[b]
$R_{P=O}$	1.470	1.467	1.52
R_{P-O}	1.589	1.589	1.57−1.58
R_{O-H}	0.965	0.964	0.9−1.1
$\theta_{O=P-O}$	116.3	116.2	112
θ_{O-P-O}	101.9	102.0	105

[a] Calculated with the aug-cc-pV(T+d)Z basis set. [b] From ref 52.

structure of H_3PO_4 determined by X-ray diffraction.[52] We find the P−O and O−H bond lengths to be very similar to the experimental values, with the calculated double bond P=O shorter by 0.05 Å. The calculated and experimental bond angles differ by a few degrees. These differences are expected when comparing with an X-ray structure.

We have also identified a second slightly higher energy conformer of H_3PO_4 in which one of the hydroxyl groups is pointing away from the P=O group. This conformer has C_1 symmetry and is illustrated in Figure 1b. We find that the calculated CCSD(T)/aug-cc-pV(T+d)Z electronic energy difference between the two conformers is 1.5 kcal mol^{-1}. The structural degeneracy of the C_1 structure is 6, and that of the C_3 structure is 2. Thus, at room temperature, only ~20% of phosphoric acid molecules will have the C_1 structure. At higher altitudes, where the temperature is lower, the C_1 conformer will be even less abundant, and we have not considered this conformer further. Furthermore, the vibrational and electronic spectra of the C_1 conformer are probably very similar to those of the C_3 conformer.

The largest correlation consistent basis set that is practicable for H_3PO_4 with the CCSD(T) method is the aug-cc-pV(T+d)Z basis set. To ensure that this basis set is suitable for calculating the structure and properties of H_3PO_4, we have examined two smaller molecules, OPH_3 and PH_2OH, with the CCSD(T) method and a large range of correlation consistent basis sets. These two molecules are small enough that large basis sets can be used with the CCSD(T) method and give a good estimation of the descriptions of P=O and P−O−H bonds. We find that the CCSD(T)/aug-cc-pV(T+d)Z geometries of OPH_3 and PH_2OH are in good agreement with CCSD(T) geometry obtained with larger quadruple- and pentuple-ζ basis sets and with experimental values (see Supporting Information, Table S1).

Photodissociation of Phosphoric Acid

The fate of phosphoric acid in the atmosphere is key to understanding the role of volatile phosphorus compounds in the atmosphere. We have calculated the energetics of all sensible unimolecular dissociation reactions of phosphoric acid (see Supporting Information, Table S2) and find that

$$H_3PO_4 + h\nu \rightarrow HOPO_2 + H_2O \qquad (4)$$

has by far the lowest activation energy. The stationary points and energetics for this reaction are presented in Figure 2. We find that the reaction proceeds through a single transition state. In the transition state, the OH group is rotated so that the hydrogen atom is directed toward one of the neighboring oxygen atoms and both the O−H bond of the rotating hydrogen and the P−O bond of the leaving oxygen are elongated. The transition state for H_3PO_4 is similar to that found for the dehydration reaction of H_2SO_4 ($H_2SO_4 \rightarrow H_2O + SO_3$).[53] The energy barrier for the dissociation of H_3PO_4 is $\Delta_f G_{298K} = 48.2$ kcal mol^{-1}, as shown in Table 2 (see Supporting Information, Tables S3 and S4, for details). This activation energy is higher than but similar to that of the H_2SO_4 dissociation,[17] for which we calculate the energy barrier with the CCSD(T)/aug-cc-pV(T+d)Z method and MP2/aug-cc-pV(T+d)Z thermodynamic correction to be $\Delta_f G_{298K} = 36.0$ kcal mol^{-1}.

Fundamental Vibrational Transitions

In Table 3, we compare harmonic frequencies and intensities and VPT2 frequencies of H_3PO_4 with room temperature Raman spectra of aqueous H_3PO_4.[54] Somewhat surprisingly, harmonic frequencies calculated with the MP2/aug-cc-pV(T+d)Z method are quite close to those calculated with the CCSD(T)/aug-cc-pV(T+d)Z method. To our knowledge, vibrational spectra of H_3PO_4 have been recorded only for aqueous solutions and in the crystal phase.[54] The assignment of the experimental vibrational modes follows the work of Preston et al.[55] and Chapman et al.[56] Obviously, we expect only partial agreement between our calculated gas phase transitions and the experimental aqueous phase spectra because of intermolecular hydrogen bonding and solution effects. The calculated VPT2 wavenumbers differ from the experimental wavenumbers by 50−150 cm^{-1}. The P−O stretching vibrational mode of A symmetry is the only transition that has been measured in several aqueous solution and solid-phase experiments.[54−58] The absorption of this mode is concentration-dependent, with the band observed in a wavenumber range of 840−960 cm^{-1}.[54,55] The VPT2 calculated anharmonic wavenumber is 843 cm^{-1} and lies in the lower limit of this range.

Local Mode OH-Stretching Transitions

The energy barrier for the dissociation reaction in eq 4 is modest and may be overcome by absorption of energy via an

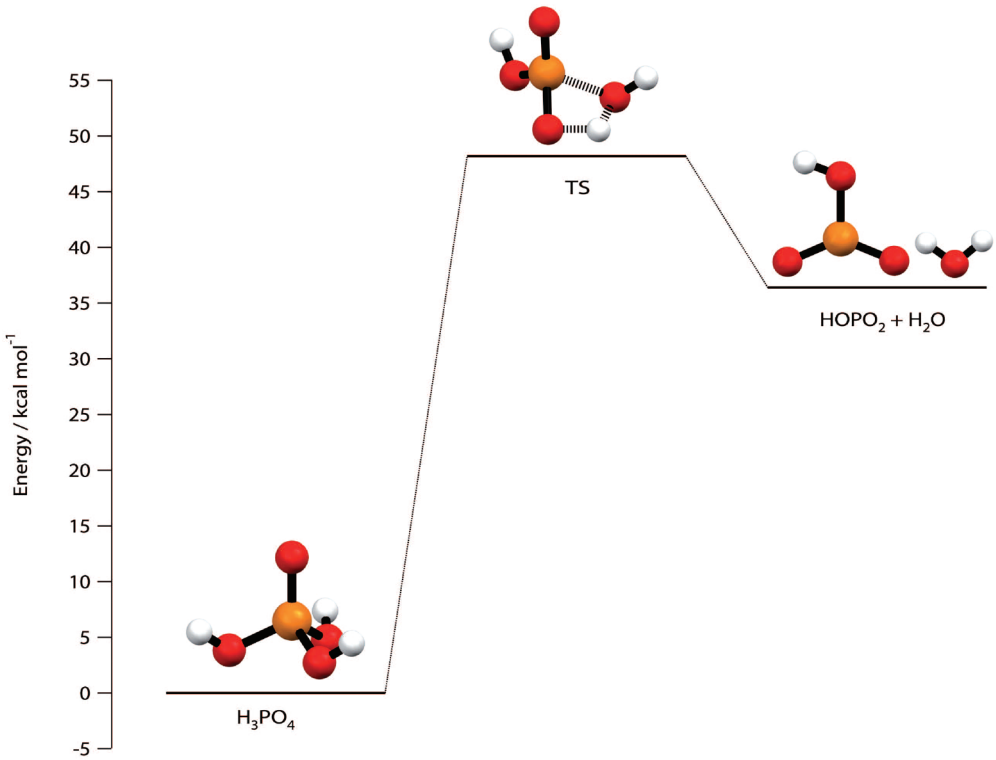

Figure 2. Energies ($\Delta_f G_{298K}$) of the stationary points on the reaction pathway for the dissociation of H_3PO_4. Calculated with CCSD(T)/CBS energies and MP2/aug-cc-pV(T+d)Z thermodynamic correction.

TABLE 2: Activation Energy (in kcal mol^{-1}) Dissociation of H_3PO_4

electronic energy	50.4[a]
electronic energy + ZPVE	48.4[b]
$\Delta_f H_{298K}$	47.9[c]
$\Delta_f G_{298K}$	48.2[c]

[a] CCSD(T)/CBS energy. [b] CCSD(T)/CBS energy including ZPVE correction calculated with MP2/aug-cc-pV(T+d)Z harmonic frequencies. [c] CCSD(T)/CBS electronic energy with a MP2/aug-cc-pV(T+d)Z thermodynamic correction at 298 K.

TABLE 3: Vibrational Frequencies (in cm^{-1}) and IR (in km mol^{-1}) and Raman Intensities (in Å^4 /AMU) of H_3PO_4

harmonic oscillator							
$\tilde{\nu}^a$	$\tilde{\nu}^b$	IR int.[b]	Raman int.[b]	VPT2 $\tilde{\nu}^b$	exptl $\tilde{\nu}^c$	symm.	assignment
3841	3840	25	135	3668		*A*	OH stretch
3838	3838	407	51	3665		*E*	OH stretch
1328	1322	300	12	1314	1170	*A*	P=O stretch
1062	1054	120	3	1021		*E*	POH bend
1054	1043	88	2	1015		*A*	POH bend
945	939	658	2	917	1010	*E*	P−O stretch
857	856	17	26	843	892	*A*	P−O stretch
463	461	124	3	455	498	*E*	OPO bend
458	455	15	1	427	498	*A*	OPO bend
381	380	86	1	346	370	*E*	twist
320	315	82	0.2	214		*A*	twist
170	166	134	3	112		*E*	OH wag

[a] Calculated with the CCSD(T)/aug-cc-pV(T+d)Z method. [b] Calculated with the MP2/aug-cc-pV(T+d)Z method. [c] From ref 54.

OH-stretching overtone transition. The atmospheric importance of OH-stretching overtone-induced photodissociation reactions has been shown for sulfuric acid,[59] hydrogen peroxide,[60−62] nitric acid,[63,64] peroxynitrous acid,[64−67] and hydroxymethyl hydroperoxide.[68] The CCSD(T)/aug-cc-pV(T+d)Z calculated local mode parameters for the OH-stretching vibrations of H_3PO_4 are $\tilde{\omega}$ = 3842 cm^{-1} and $\tilde{\omega}x$ = 79.56 cm^{-1}. The calculated local mode harmonic wavenumber, 3842 cm^{-1}, is very close to the calculated CCSD(T)/aug-cc-pV(T+d)Z harmonic normal mode OH-stretching wavenumbers of 3841 and 3838 cm^{-1}. This small difference of only a few wavenumbers illustrates that the OH-stretching vibrational mode is well described by the local mode model.[31] Furthermore, the small splitting between the two OH-stretching normal modes frequencies indicates very small coupling between the two OH-stretching local modes, of similar magnitude to the coupling between the two OH-stretching vibrations in H_2O_2.[69]

TABLE 4: Calculated OH-Stretching Frequencies (in cm^{-1}) and Oscillator Strengths of H_3PO_4, Using the 1-D Local-Mode Model

	Morse[a]		numeric[b]		numeric[c]
state	$\tilde{\nu}$	*f*	$\tilde{\nu}$	*f*	$\tilde{\nu}$
1	3 683	5.6×10^{-5}	3 686	5.5×10^{-5}	3 790
2	7 207	1.7×10^{-6}	7 217	1.9×10^{-6}	7 394
3	10 572	4.4×10^{-8}	10 597	6.3×10^{-8}	10 800
4	13 777	2.2×10^{-9}	13 827	4.2×10^{-9}	13 999
5	16 824	1.9×10^{-10}	16 911	4.6×10^{-10}	16 999
6	19 711	2.6×10^{-11}	19 848	7.1×10^{-11}	19 826
7	22 440	4.6×10^{-12}	22 640	1.4×10^{-11}	22 521

[a] Calculated with a CCSD(T)/aug-cc-pV(T+d)Z dipole moment function and local mode parameters: $\tilde{\omega}$ = 3842 cm^{-1} and $\tilde{\omega}x$ = 79 cm^{-1}. [b] Calculated with a CCSD(T)/aug-cc-pV(T+d)Z dipole moment function and a numeric potential. [c] Calculated with a PM3 numeric potential.

In Table 4, we present the calculated frequency and oscillator strength of the local mode OH-stretching overtone transitions obtained with Morse and numerical potentials. For the fundamental transition, the frequency and the intensity calculated with the two approaches is virtually the same. The frequencies and oscillator strengths calculated with the two approaches diverge with increasing Δv, with the numeric solution at higher energy

TABLE 5: Number of Simulated Trajectories and Time Scale (in ps) of the $H_3PO_4 \rightarrow HOPO_2 + H_2O$ Dissociation Events[a]

	type−OH		type−OH + POH	
υ	N[b]	T[c]	N[b]	T[c]
5	0/32		23/48	0.1−25 (∼0.1−0.2)
6	0/32		30/48	0.1−39 (∼0.1)
7	7/32	0.5−66 (∼ 1)	39/48	0.1−21 (∼0.1−0.5)

[a] Calculated with the CC-VSCF/PM3 method. [b] Dissociation events/total trajectories tested. [c] Range of times with typical time in parentheses.

and higher intensity. Because the OH-stretching overtone transitions of H_3PO_4 are yet to be experimentally recorded, it is not clear which of the two methods is more accurate. For H_2SO_4, vibrational frequencies calculated using a Morse potential were found to be slightly closer to experiment than vibrational frequencies calculated using a numeric potential. The Morse calculated OH-stretching oscillator strengths of H_2SO_4 were found to be slightly lower than experiment, whereas the numeric calculated oscillator strengths were found to be slightly higher than experiment.[18]

Overtone-Induced Photodissociation Dynamics

The activation energy for the photodissociation of H_3PO_4 (eq 4) is 48.2 kcal mol^{-1}. Excitation of the rotationless fourth overtone ($\upsilon = 5$) OH-stretching transition provides 48.3 kcal mol^{-1} (∼16900 cm^{-1}). Hence, photodissociation of H_3PO_4 excited to $\upsilon = 5$, promoted by rotational energy, and higher vibrational levels are expected to occur. To examine the probability of the proposed overtone-induced photodissociation of H_3PO_4, we have performed classical trajectory simulations.[39] The OH-stretching overtone transitions frequencies calculated with the PM3 method within the local mode model are presented in Table 4 for comparison with the higher-quality calculations. The activation energy of the photodissociation reaction of H_3PO_4 calculated with the PM3 method is somewhat lower than the one calculated by other methods and is $\Delta_f G_{298K} = 41.5$ kcal mol^{-1} (∼15000 cm^{-1}) (see Supporting Information, Table S4). This underestimate of the activation energy will likely give a larger number of dissociative trajectories than would be obtained with higher level ab initio methods. Nonetheless, the PM3 results should still provide qualitative answers to whether the reaction will proceed and the time frame for dissociation events.

In Table 5, we show the number of simulated trajectories, which yield dissociation of H_3PO_4 into $HOPO_2$ and H_2O. We have computed trajectories corresponding to excitation of the pure OH-stretching overtone mode (type−OH) and to excitation of combination modes with υ quanta in the OH-stretching plus one quantum in the POH bending mode (type−OH + POH). In the type−OH mode simulations, none of the 32 calculated trajectories show dissociation for excitation to the $\upsilon = 5$ and 6 vibrational states, whereas for the $\upsilon = 7$ vibrational state, 22% of the trajectories lead to a dissociation event. We find that dissociation is more probable with excitation of the type−OH + POH combination states as compared to the type−OH pure overtone states. In the combination mode simulations, dissociation events are observed already for the $\upsilon = 5$ vibrational state with a 48% yield out of the 48 simulated trajectories. This percentage increases with increasing OH-stretch vibrational number up to 81% for $\upsilon = 7$ OH-stretching state.

The time scale for all successful simulated dissociations is in the range 0.1−66 ps (see Supporting Information, Tables S5 and S6). This time scale is much shorter than the mean time between collisions in the atmosphere, which is ∼10 ns at sea level and increases to a few milliseconds at high altitudes. Thus, the dissociation events are likely to take place before energy loss via collision is possible. Snapshots taken at different times in a representative trajectory leading to dissociation are shown in Figure 3. The snapshots are chosen when a significant change in geometry occurs. The time frame of these successful dissociation events in H_3PO_4 is similar to the reported dissociation time of 9 ps for H_2SO_4.[42] One significant difference from the dissociation of H_2SO_4 is the lack of hydrogen-hopping in the dissociation of H_3PO_4. In all of the trajectories we have simulated, the hydrogen atoms stay close to the oxygen atoms where they originated.

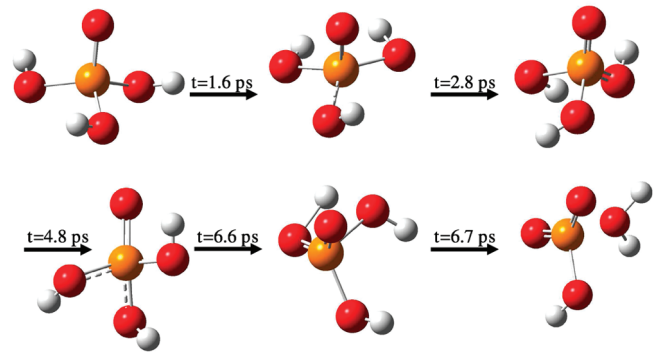

Figure 3. Snapshots from a successful dissociation event of the reaction $H_3PO_4 \rightarrow HOPO_2 + H_2O$. The $\upsilon = 7$ OH-stretching plus $\upsilon = 1$ POH bending combination state was excited. The times on the arrows are the elapsed time from start, such that the complete dissociation event took 6.7 ps.

Electronic Transitions

Phosphoric acid has a nonabelian symmetry point group, and hence, electronic excited states calculations were carried out using C_1 symmetry, but the results are analyzed and presented within the C_3 framework. Phosphoric acid has a total of 23 valence molecular orbitals (MOs), of which 16 are occupied and 7 are unoccupied (virtual). The electronic configuration of H_3PO_4 is

$$(\text{core})^{18}6a^2 3e^4 7a^2 8a^2 4e^4 9a^2 5e^4 6e^4 10a^2 11a^2 7e^4 12a^0 8e^0 13a^0 14a^0 9e^0$$

where a and e are the symmetries of the MOs and the superscripts 0, 2, and 4 are the number of electrons in each MO.

In Table 6, we compare the lowest energy excited states of H_3PO_4 calculated with the EOM-CCSD method using the aug-cc-pV(T+d)Z and aug-cc-pV(T+d)Z+5 basis sets. For the lower energy states, there is little variation in the vertical excitation energies obtained with the two sets. However, for the higher energy states, the effect of the additional highly diffuse basis functions is significant, with vertical excitation energy lowered by up to 0.5 eV. This variation in the vertical excitation energies of the higher states with increasing number of diffuse basis functions is consistent with the previous calculation for H_2SO_4 and suggests significant Rydberg character of these states.[51]

The EOM-CCSD method has been shown to be reasonably well converged with respect to including higher-order excitation for excited states dominated by single excitations and gives results similar to those calculated by a third-order approximate coupled cluster singles, doubles, and triples (CC3) method.[51,70]

TABLE 6: EOM-CCSD Vertical Excitation Energies (in eV) and Oscillator Strengths of the Electronic Transitions in H_3PO_4

	aug-cc-pV(T+d)Z		aug-cc-pV(T+d)Z+5	
	E	*f*	*E*	*f*
^{1}A	8.748	0.0168	8.737	0.0153
^{1}A	9.041	0.0000	9.005	0.0000
^{1}A	9.152	0.0044	9.122	0.0060
^{1}A	9.919	0.1051	9.866	0.0921
^{1}A	10.283	0.0005	9.936	0.0018
^{1}A	10.373	0.0027	10.001	0.0221
^{1}A	10.669	0.0120	10.196	0.0151
^{1}A			10.225	0.0004
^{1}A			10.357	0.0000
^{1}A			10.406	0.0000
^{1}E	7.785	0.0634	7.782	0.0640
^{1}E	8.889	0.0117	8.860	0.0100
^{1}E	9.623	0.1178	9.522	0.0529
^{1}E	9.847	0.0172	9.671	0.0620
^{1}E	10.304	0.0037	9.962	0.0090
^{1}E	10.379	0.0539	9.993	0.0230
^{1}E			10.169	0.0146
^{1}E			10.208	0.0005
^{1}E			10.350	0.0011

For completeness, we also calculate vertical excitation energies and oscillator strengths with the coupled cluster singles (CCS) and second order approximate coupled cluster singles and doubles (CC2) methods (see Supporting Information, Table S7). We find that the variation between vertical excitation energies calculated by the different coupled cluster methods is similar to the variation observed in previous calculations for H_2SO_4.[51]

We have also calculated the lowest-lying triplet excited states of H_3PO_4 with the EOM-CCSD/aug-cc-pV(T+d)Z+5 method and find the lowest vertical excitation energy to be 7.60 eV. We are unable to calculate oscillator strengths for these spin-forbidden transitions. The intensities of spin-forbidden transitions are inherently weaker than the intensity of spin-allowed transitions, and we have not included these when calculating the electronic cross section. However, for H_3PO_4, the lowest triplet state is close in energy to the first excited singlet state. Therefore, the spin-forbidden transition might "borrow" some intensity from the spin-allowed $S_0 \rightarrow S_1$ transition via spin−orbit coupling. The contribution to the total cross section will be small but still finite and requires further investigation.

We are not aware of any previous theoretical investigation of the electronic spectroscopy of H_3PO_4, and there have been only limited experimental investigations. The vapor phase electronic absorption spectra of H_3PO_4 were reported in 1939 and show a diffuse band at 5.1 eV.[71] This absorption band is significantly lower in energy than our lowest calculated state. The accuracy of our present calculated electronic transitions is conservatively estimated to be ∼0.3 eV (based on coupled cluster method convergence and basis set convergence[51]), and we believe this early experimental result to be incorrect.

In 1965, Halmann and Platzner[72] recorded electronic absorption spectra of aqueous solutions of phosphoric acid in the range from 6.0 to 6.8 eV. They were unable to identify any absorption feature due to H_3PO_4, and the dominant features in their spectra were attributed to the dihydrogen phosphate ion $H_2PO_4^-$, with an absorption around 6.5−6.8 eV. We calculated the low-lying electronic excited states of $H_2PO_4^-$ with the polarized continuum model to approximate the solvent effect using the time dependent density functional theory calculations with the B3LYP functional and the aug-cc-pV(T+d)Z basis set. The energies of the first six electronic transitions are calculated to be between 6.1 and 6.5 eV, showing a reasonable agreement with the observed spectra.

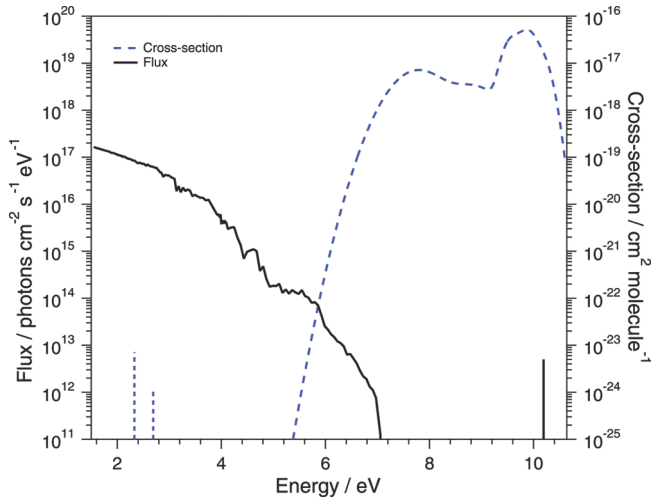

Figure 4. Simulated absorption cross section of H_3PO_4 and the solar flux at 80 km.

Each electronic transition has been convoluted with a Gaussian band profile with a half width at half-maximum (HWHM) of 0.47 eV for the transitions below 9.5 and a HWHM of 0.15 eV for the higher energy transitions. These band widths are derived from experimental spectra of SO_3[73,74] and SO_2,[75] and we assume those of H_3PO_4 to be somewhat comparable.

Our simulated spectrum indicates a large cross section of 1.7×10^{-17} cm^2 molecule^{-1} for H_3PO_4 in the region of the Lyman-α radiation (∼10.2 eV). The accuracy of this cross section depends on several variables, including the absolute vertical excitation energies and oscillator strengths and the bandwidth used for convolution. We estimate that the calculated vertical excitation energies for H_3PO_4 in the Lyman-α region are within ∼0.1 eV of the actual values. If we blue or redshift the calculated vertical excitation energies by 0.1 eV, the cross section becomes 2.8×10^{-17} and 8.5×10^{-18} cm^2 molecule^{-1}, respectively, in the Lyman-α region. We estimate the error of our calculated oscillator strength to be within a factor of 2; hence, if we double or halve the calculated oscillator strengths, the cross section at Lyman-α becomes 3.3×10^{-17} and 8.3×10^{-18} cm^2 molecule^{-1}, respectively. The bandwidth of the lower energy transitions does not affect the cross section at Lyman-α. If we double or halve the 0.15 eV (1210 cm^{-1}) HWHM of the high energy transitions used to convolute the spectra, the cross section coincidentally becomes 2.0×10^{-17} cm^2 molecule^{-1} in both cases. In summary, we estimate the cross section of H_3PO_4 in the Lyman-α region to be in the range 8×10^{-18} to 3×10^{-17} cm^2 molecule^{-1}.

Atmospheric Photodissociation Rate Constants

The photodissociation rate constant (J) for H_3PO_4 can be calculated using the following equation,

$$J = \int I(\nu)\, \Phi(\nu)\, \sigma(\nu)\, d\nu \qquad (5)$$

where $I(\nu)$ is the frequency-dependent solar flux, $\Phi(\nu)$ is the quantum yield, and $\sigma(\nu)$ is the cross section.[76]

In Figure 4, we present the cross section for H_3PO_4 and the solar flux at 80 km in the visible, UV, and Lyman-α regions. The cross section in the visible region around 2−2.5 eV corresponds to absorption via the $\Delta v_{OH} = 5$ and 6 vibrational transitions. The cross section in the UV region corresponds to

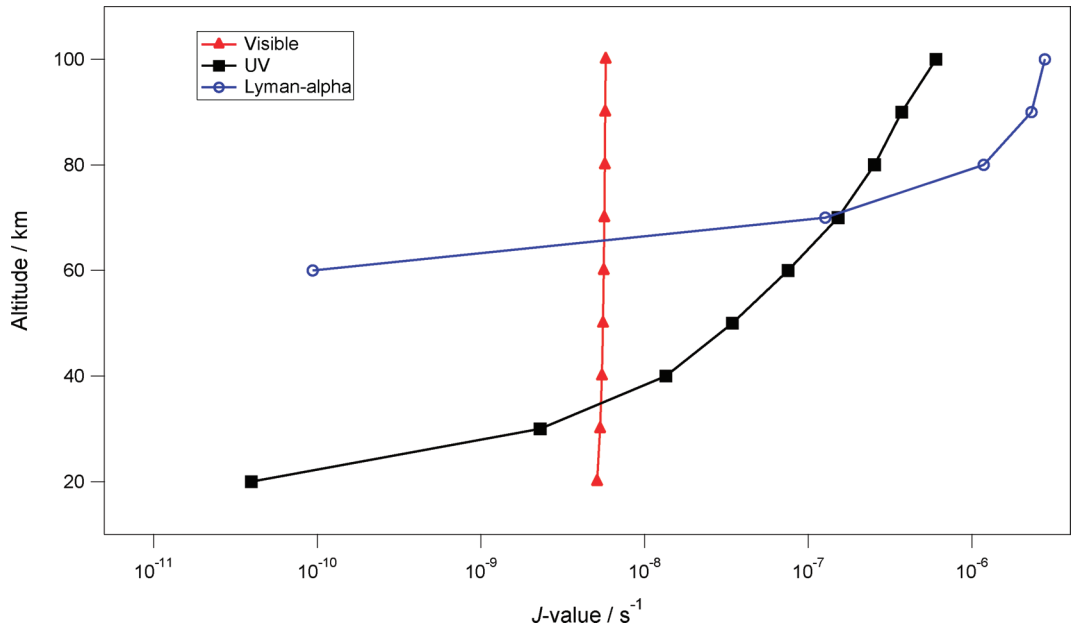

Figure 5. Photodissociation rate constants for H_3PO_4 in the atmosphere.

the absorption of the calculated low-energy valence electronic transitions, whereas the cross section in the Lyman-α region corresponds to absorption of the high energy Rydberg electronic transitions. We use the TUV radiation model[77] to calculate the solar flux from 120 to 800 nm (1.55−10.3 eV). The calculated flux is averaged over a 24 h period, for 26° N to 32° N, over two days in April and two days in May. These conditions are similar to those used previously by Mills et al.[78] As seen in Figure 4, the H_3PO_4 cross section in the visible region is limited to a very small, narrow band while the flux of solar photons is high. Conversely, in the region of Lyman-α radiation, the cross section of H_3PO_4 is very large and the flux of solar photons is small and limited to a narrow region. In the UV region, both the cross section of H_3PO_4 and the flux are reasonably small, but they overlap in a large region of ∼2 eV. The flux of photons in the visible region is more or less constant over all altitudes, whereas the flux of photons in the UV and Lyman-α regions is strongly dependent on altitude.[76] It follows that the dominant mechanism for H_3PO_4 is likely to depend on the altitude of reaction.

In Figure 5, we present the *J* values for photodissociation of H_3PO_4 calculated at altitudes of 20−100 km. The visible *J* values correspond to the OH-stretching overtone induced photodissociation mechanism, using an integrated cross section for $\Delta v_{OH} = 5$ and 6, for which the OH-stretching overtone transition was convoluted with a Gaussian band profile with a fwhm of 54 cm^{-1}. This bandwidth is derived from experimental spectra of H_2SO_4,[79] and we assume that of H_3PO_4 to be comparable. The UV *J* values correspond to photodissociation in the UV region (160−220 nm, 5.6−7.8 eV), using the cross section in the low-energy region of the simulated spectra (Figure 4) obtained with the calculated EOM-CCSD/aug-cc-pV(T+d)Z+5 lower energy electronic transitions. The Lyman-α *J* values correspond to the photodissociation by Lyman-α photons, using the cross section of the simulated spectrum obtained with the calculated EOM-CCSD/aug-cc-pV(T+d)Z+5 electronic transitions in the region of the Lyman-α radiation (∼10.2 eV). We assume a quantum yield of 1 for all suggested mechanisms at all altitudes. A quantum yield of less than 1 will lower the *J* values, which is more likely for the OH-stretching overtone induced mechanism because the relevant absorption energy is close to the energy required for dissociation.

At altitudes below 30 km, there is a large flux in the visible region, and hence, the *J* values from overtone transitions are several orders of magnitude greater than those for the UV and Lyman-α photodissociation mechanisms. The dynamics of the OH-stretching overtone induced photodissociation of H_3PO_4 have been estimated with DRC simulations. The probability of an overtone-induced dissociation event is ∼50% when an OH-stretching plus POH bending combination state is excited. This is not a full estimation of the quantum yield of this process at different altitudes, but it suggests that the actual *J* values are likely lower than the upper limits of *J* values given here. However, at these altitudes, H_3PO_4 is unlikely to exist as molecules, but would probably be hydrated to some extent within aerosols.

From 40 to 100 km, the solar flux and, hence, the *J* value for the UV photodissociation mechanism increases by 2 orders of magnitude. The cross section of H_3PO_4 is relatively small in the UV region, but there is still significant overlap with the actinic flux, particularly at altitudes higher than 30 km. Hence, above 30 km, the UV *J* value is larger than that from overtone transitions. Obviously, reducing the quantum yield of the OH-stretching mechanism would decrease the *J* values for the visible radiation mechanism even further. This may mean that the UV photodissociation mechanism dominates at even lower altitudes than indicated in Figure 5. In addition, the lower-energy, spin-forbidden, singlet−triplet transitions may contribute to the low-energy tail of the cross section in the UV region, resulting in an even larger overlap with the actinic flux. The calculated *J* values for the UV and Lyman-α photodissociation mechanisms are approximately equivalent at 70 km altitude. At altitudes above 70 km, the calculated *J* values for the Lyman-α photodissociation mechanism are up to 5 times greater than *J* values for the UV photodissociation mechanism.

In summary, we find that at altitudes below 30 km, photodissociation of H_3PO_4 is likely to occur via the visible radiation OH-stretching overtone induced photodissociation mechanism. However, due to the large concentration of water molecules in the troposphere, phosphoric acid at these altitudes is likely to

exist as part of an aerosol, for which the dissociation mechanism is likely different and is outside of the scope of this investigation. At 30−70 km altitude, electronic transitions in the UV region are likely to be responsible for photodissociation of H_3PO_4. At altitudes above 70 km, the Lyman-α mechanism yields J values that are about 2−5 times bigger than those corresponding to the UV mechanism. This suggests that it is important to measure the electronic absorption of gaseous phosphoric acid, including excitations to singlet and to low-lying triplet states. In addition, to achieve a better description of the J values of H_3PO_4, the intensity of the spin-forbidden excitations of H_3PO_4 should be evaluated theoretically.

Conclusions

We have optimized the ground state structure of H_3PO_4 using the CCSD(T)/aug-cc-pV(T+d)Z method. We have calculated all sensible unimolecular dissociation reactions of H_3PO_4 and find the reaction forming $HOPO_2$ and H_2O to be the only likely dissociation with an energy barrier of 48 kcal mol^{-1}. We have calculated the fundamental vibrational transitions and the OH-stretching fundamental and overtone transitions. We have estimated the probability of the dissociation event of H_3PO_4 into $HOPO_2$ and H_2O using "on the fly" dynamical reaction coordinate simulations with the PM3 method and showed that OH-stretching overtone induced photodissociation of H_3PO_4 is a viable dissociation process. We have also calculated electronic transitions for H_3PO_4 and simulated the electronic absorption cross section. Finally, we have calculated the photodissociation rate constants (J values) for absorption of visible, UV and Lyman-α radiation at 20−100 km altitudes. At altitudes between 30 and 70 km, where phosphoric acid might exist in a gaseous form, we find that photodissociation is likely to proceed via absorption in the UV region. At altitudes higher than 70 km, we find that photodissociation of H_3PO_4 is likely to proceed via absorption in the Lyman-α region.

Acknowledgment. We thank Anna Garden, Keith Hunter, Isobel Maxwell-Cameron, and Yifat Miller for helpful discussions, and we acknowledge the Marsden Fund administered by the Royal Society of New Zealand for financial support.

Supporting Information Available: Selected geometric parameters calculated with the CCSD(T) method and different correlation consistent basis set for OPH_3 and H_2POH. Energy difference between products and reactants for unimolecular dissociation reaction of H_3PO_4 calculated with MP2/aug-cc-pV(T+d)Z. Comparison of energy values of the reactant, products, and transition state of the photodissociation reaction of H_3PO_4. Activation energy and energy difference between products and reactant for H_3PO_4 dissociation. Vertical excitation energies and oscillator strengths for the electronic transitions in H_3PO_4. This material is available free of charge via the Internet at http://pubs.acs.org.

References and Notes

(1) Westheimer, F. H. *Science* **1987**, *235*, 1173.
(2) Graham, W. F.; Duce, R. A. *Geochim. Cosmochim. Acta* **1979**, *43*, 1195.
(3) Schink, B.; Friedrich, M. *Nature* **2000**, *406*, 37.
(4) Marinov, I.; Gnanadesikau, A.; Toggweiler, J. R.; Sarmiento, J. L. *Nature* **2006**, *441*, 964.
(5) Deutsch, C.; Sarmiento, J. L.; Sigman, D. M.; Gruber, N.; Dunne, J. P. *Nature* **2007**, *445*, 163.
(6) Glindemann, D.; Edwards, M.; Kuschk, P. *Atmos. Environ.* **2003**, *37*, 2429.
(7) Glindemann, D.; Bergmann, A.; Stottmeister, U.; Gassmann, G. *Naturwissenschaften* **1996**, *83*, 131.
(8) Gassmann, G.; Glindemann, D. *Angew. Chem., Int. Ed. Engl.* **1993**, *32*, 761.
(9) Morton, S. Y.; Edwards, M. *Crit. Rev. Environ. Sci. Technol.* **2005**, *35*, 333.
(10) Zhu, R.; Kong, D.; Sun, L.; Geng, J.; Wang, X.; Glindemann, D. *Environ. Sci. Technol.* **2006**, *40*, 7656.
(11) Han, S.; Zhuang, Y.; Liu, J.; Glindemann, D. *Sci. Total Environ.* **2000**, *258*, 195.
(12) Liu, J.; Yahui, C. H. Z.; Kuschk, P.; Eismann, F.; Glindemann, D. *Water Air Soil Pollut.* **1999**, *116*, 597.
(13) Dumas, T. *J. Agric. Food Chem.* **1980**, *28*, 337.
(14) Gupta, P.; Yekutiel, M.; Lane, J. R.; Kjaergaard, H. G. Unpublished work.
(15) Schlager, N.; Weisblatt, J.; Newton, D. E. *Chemical Compounds*; Thomson Gale: Detroit, 2006.
(16) Burkholder, J. B.; Mills, M.; Mckeen, S. *Geophys. Res. Lett.* **2000**, *27*, 2493.
(17) Vaida, V.; Kjaergaard, H. G.; Hintze, P. E.; Donaldson, D. J. *Science* **2003**, *299*, 1566.
(18) Kjaergaard, H. G.; Lane, J. R.; Garden, A. L.; Schofield, D. P.; Robinson, T. W.; Mills, M. J. *Adv. Quantum Chem.* **2008**, *55*, 137.
(19) Werner, H.-J.; Knowles, P. J.; Lindh R.; Manby, F.c R.; Celani, M. S. P.; Korona T.; Rauhut, G.; Amos, R. D.; Bernhardsson, A.; Berning, A.; Cooper, D. L.; Deegan, M. J. O.; Dobbyn, A. J.; Eckert, F.; Hampel, C.; Hetzer, G.; Lloyd, A. W.; McNicholas, S. J.; Meyer, W.; Mura, M. E.; Nicklass, A.; Palmieri, P.; Pitzer, R.; Schumann, U.; Stoll, H.; Stone, A. J.; Tarroni, R.; Thorsteinsson, T. *MOLPRO, version 2006.1, a package of ab initio programs*, 2006.
(20) Helgaker, T.; Jørgensen, P.; Olsen, J. *Molecular Electronic Structure Theory*; John Wiley and Sons, Ltd.: Chichester, England, 2000.
(21) Halkier, A. J.; Helgaker, T.; Jørgensen, P.; Klopper, H.; Koch, H.; Olsen, J.; Wilson, A. K. *Chem. Phys. Lett.* **1998**, *286*, 243.
(22) Mills, I. M. In *Modern Spectroscopy: Modern Research*; Rao, K. N., Matthews, C. W., Eds.; Academic Press: New York, 1972; page 115.
(23) Frisch, M.; Trucks, G.; Schlegel, H.; Scuseria, G.; Robb, M.; Cheeseman, J., Jr.; Vreven, J. M.; Kudin, T.; Burant, K.; Millam, J.; Iyengar, J.; Tomasi, S.; Barone, J.; Mennucci, V.; Cossi, B.; Scalmani, M.; Rega, G.; Petersson, N.; Nakatsuji, G.; Hada, H.; Ehara, M.; Toyota, M.; Fukuda, K.; Hasegawa, R.; Ishida, J.; Nakajima, M.; Honda, T.; Kitao, Y.; Nakai, O.; Klene, H.; Li, M.; Knox, X.; Hratchian, J.; Cross, H.; Bakken, J.; Adamo, V.; Jaramillo, C.; Gomperts, J.; Stratmann, R.; Yazyev, R.; Austin, O.; Cammi, A.; Pomelli, R.; Ochterski, C.; Ayala, J.; Morokuma, P.; Voth, K.; Salvador, G.; Dannenberg, P.; Zakrzewski, J.; Dapprich, V.; Daniels, S.; Strain, A.; Farkas, M.; Malick, O.; Rabuck, D.; Raghavachari, A.; Foresman, K.; Ortiz, J.; Cui, J.; Baboul, Q.; Clifford, A.; Cioslowski, S.; Stefanov, J.; Liu, B.; Liashenko, G.; Piskorz, A.; Komaromi, P.; Martin, I.; Fox, R.; Keith, D.; Al-Laham, T.; Peng, M.; Nanayakkara, C.; Challacombe, A.; Gill, M.; Johnson, P.; Chen, B.; Wong, W.; Gonzalez, M.; Pople, C. *Gaussian 03, Revision E.01*; Gaussian Inc.: Wallingford, CT, 2004.
(24) Henry, B. R.; Kjaergaard, H. G. *Can. J. Chem.* **2002**, *80*, 1635.
(25) Tarr, A. W.; F., Z. *Chem. Phys. Lett.* **1989**, *154*, 273.
(26) Donaldson, D. J.; Orlando, J. J.; Amann, S.; Tyndall, G. S.; Pross, R. J.; Henry, B. R.; Vaida, V. *J. Phys. Chem.* **1989**, *102*, 5171.
(27) Kjaergaard, H. G. *J. Phys. Chem. A.* **2002**, *106*, 2979.
(28) Howard, D. L.; Kjaergaard, H. G. *J. Chem. Phys.* **2004**, *121*, 136.
(29) Schofield, D. P.; Lane, J. R.; Kjaergaard, H. G. *J. Phys. Chem. A* **2007**, *111*, 567.
(30) Watson, I. A.; Henry, B. R.; Ross, I. G. *Spectrochim. Acta* **1981**, *37A*, 857.
(31) Howard, D. L.; Jørgensen, P.; Kjaergaard, H. G. *J. Am. Chem. Soc.* **2005**, *127*, 17096.
(32) Herzberg, G. *Molecular Spectra and Molecular Structure I. Spectra of Diatomic Molecules* D. Van Nostrand Company, Inc.: Princton, NJ, 1950.
(33) Kjaergaard, H. G.; Henry, B. R. *J. Chem. Phys.* **1992**, *96*, 4841.
(34) Low, G. R.; Kjaergaard, H. G. *J. Chem. Phys.* **1999**, *110*, 9104.
(35) Olsen, J."Onedim program", Private communication, 2005.
(36) Lane, J. R.; Kjaergaard, H. G. *J. Phys. Chem. A* **2007**, *111*, 9707.
(37) Atkins, P. W.; Friedman, R. S. *Molecular Quantum Mechanics*, 3rd ed.; Oxford University Press: Oxford, 1997.
(38) Kjaergaard, H. G.; Yu, H.; Schattka, B. J.; Henry, B. R.; Tarr, A. W. *J. Chem. Phys.* **1990**, *93*, 6239.
(39) Stewart, J. J. P.; Davis, L. P.; Burggraf, L. W. *J. Comput. Chem.* **1987**, *8*, 1117.
(40) Schmidt, M. W.; Baldridge, K. K.; Boatz, J. A.; Elbert, S. T.; Gordon, M. S.; Jensen, J. H.; Koseki, S.; Matsunaga, N.; Nguyen, K. A.; Su, S. J.; Windus, T. L.; Dupuis, M.; Montgomery, J. A. *J. Comput. Chem.* **1993**, *14*, 1347.
(41) Gordon, M. S.; Schmidt, M. W. Advances in electronic structure theory: GAMESS a decade later. In *Theory and Applications of Computational Chemistry, The First Forty Years*; Dykstra, C. E.; Frenking, G.; Kim, K. S.; Scuseris, G. E., Eds.; Elsevier: Amsterdam, 2005.

(42) Miller, Y.; Gerber, R. B. *J. Am. Chem. Soc.* **2006**, *128*, 9594.
(43) Miller, Y.; Chaban, G. M.; Finlayson-Pitts, B. J.; Gerber, R. B. *J. Phys. Chem. A* **2006**, *110*, 5342.
(44) Jung, J. O.; Gerber, R. B. *J. Chem. Phys.* **1996**, *105*, 10332.
(45) Chaban, G. M.; Jung, J.-O.; Gerber, R. B. *J. Chem. Phys.* **1999**, *111*, 1823.
(46) Miller, Y.; Chaban, G. M.; Gerber, R. B. *J. Phys. Chem. A* **2005**, *109*, 6565.
(47) Miller, Y.; Chaban, G. M.; Gerber, R. B. *Chem. Phys.* **2005**, *313*, 213.
(48) Stewart, J. J. *J. Comput. Chem.* **1989**, *10*, 209.
(49) Stewart, J. J. *J. Comput. Chem.* **1989**, *10*, 221.
(50) Kaufmann, K.; Baumeister, W.; Jungen, M. *J. Phys. B: At. Mol. Opt. Phys.* **1989**, *22*, 2223.
(51) Lane, J. R.; Kjaergaard, H. G. *J. Phys. Chem. A* **2008**, *112*, 4958.
(52) Furberg, S. *Acta Chem. Scand.* **1955**, *9*, 1557.
(53) Morokuma, K.; Muguruma, C. *J. Am. Chem. Soc.* **1994**, *116*, 10316.
(54) Cherif, M.; Mgaidi, A.; Ammar, N.; Vallee, G.; Walter, F. *J. Solution Chem.* **2000**, *29*, 255.
(55) Preston, C. M.; Adams, W. A. *Can. J. Spectrosc.* **1977**, *22*, 125.
(56) Chapman, A. C.; Thrilwell, L. E. *Spectrochim. Acta* **1964**, *20*, 937.
(57) Herzog, K.; Steger, E. *J. Inorg. Nucl. Chem.* **1965**, *27*, 1429.
(58) Jeppessen, M. A.; Bell, R. M. *J. Chem. Phys.* **1935**, *3*, 363.
(59) Vaida, V.; Kjaergaard, H. G.; Hintze, P. E.; Donaldson, D. J. *Science* **2003**, *299*, 1566.
(60) Rizzo, T. R.; Hayden, C. C.; Crim, F. F. *Faraday Discuss. Chem. Soc.* **1983**, *75*, 223.
(61) Scherer, N. F.; Zewaii, A. H. *J. Chem. Phys.* **1987**, *87*, 114.
(62) Ticich, T. M.; Likar, M. D.; Dubal, H. R.; Butler, L. J.; Crim, F. F. *J. Chem. Phys.* **1987**, *87*, 5820.
(63) Sinha, A.; Vander Wal, R. L.; Crim, F. F. *J. Chem. Phys.* **1990**, *92*, 401.
(64) Donaldson, D. J.; Tuck, A. F.; Vaida, V. *Phys. Chem. Earth C* **2000**, *25*, 223.
(65) Nizkorodov, S. A.; Wennberg, P. O. *J. Phys. Chem. A* **2002**, *106*, 855.
(66) Konen, I. M.; Pollack, I. B.; Li, E. X. J.; Lester, M. I.; Varner, M. E.; Stanton, J. F. *J. Chem. Phys.* **2005**, *122*, 094320.
(67) Fry, J. L.; Nizkorodov, S. A.; Okumura, M.; Roehl, C. M.; Francisco, J. S.; Wennberg, P. O. *J. Chem. Phys.* **2004**, *121*, 1432.
(68) Fry, J. L.; Matthews, J.; Lane, J. R.; Roehl, C. M.; Sinha, A.; Kjaergaard, H. G.; Wennberg, P. O. *J. Phys. Chem. A* **2006**, *110*, 7072.
(69) Kjaergaard, H. G.; Goddard, J. D.; Henry, B. R. *J. Chem. Phys.* **1991**, *95*, 5556.
(70) Crawford, T. D.; Abrams, M. L.; Lane, J. R.; Schofield, D. P.; Kjaergaard, H. G. *J. Chem. Phys.* **2006**, *125*, 204302.
(71) Ali, S. N. *Indian J. Phys.* **1939**, *13*, 309.
(72) Halmann, M.; Platzner, I. *J. Chem. Soc.* **1965**, 1440.
(73) Hintze, P. E.; Kjaergaard, H. G.; Vaida, V.; Burkholder, J. B. *J. Phys. Chem. A* **2003**, *107*, 1112.
(74) Burkholder, J. B.; McKeen, S. *Geophys. Res. Lett.* **1997**, *24*, 3201.
(75) Feng, R.; Sakai, Y.; Zheng, Y.; Cooper, G.; Brion, C. E. *J. Chem. Phys.* **2000**, *260*, 29.
(76) Seinfeld, J. H.; Pandis, S. N. *Atmospheric Chemistry and Physics: From Air Pollution to Climate Change*; John Wiley & Sons, Inc.: New York, 1998.
(77) Madronich, S.; Flocke, S.; Zeng, J.; Petropavlovskikh, I.; Lee-Taylor, J. *NCAR/ACD TUV: Tropospheric Ultraviolet-Visible model*, NCAR Atmospheric Chemistry Division (ACD): Boulder, CO, 2005.
(78) Mills, M. J.; Toon, O. B.; Vaida, V.; Hintze, P. E.; Kjaergaard, H. G.; Schofield, D. P.; Robinson, T. W. *J. Geophys. Res. Atm.* **2005**, *110*, D08201.
(79) Feierabend, K. J.; Havey, D. K.; Brown, S. S.; Vaida, V. *Chem. Phys. Lett.* **2006**, *420*, 438.

JP1007957